Received: 25 November 2017 | Revised: 18 January 2018 | Accepted: 18 January 2018

DOI: 10.1002/jrs.5354

RESEARCH ARTICLE

WILEY Journal of RAMAN SPECTROSCOPY

Material processed with 58,000-year-old grindstones from Sibudu (KwaZulu-Natal, South Africa) identified by means of Raman microspectroscopy

Marine Wojcieszak

Evolutionary Studies Institute (ESI), University of the Witwatersrand, Johannesburg 2050, South Africa

Correspondence
Marine Wojcieszak, Evolutionary Studies Institute (ESI), University of the Witwatersrand, Johannesburg 2050, South Africa.
Email: marine.wojcieszak@gmail.com

Funding information
DST-NRF Centre of Excellence in Palaeosciences

Abstract

Despite their high potential for understanding past human behaviours, the study of grindstones is limited in the literature compared with other forms of lithic tools. This paper reports the combination of optical microscopy and Raman microspectroscopy for understanding the uses of a selection of six grindstones from the post-Howiesons Poort layers at Sibudu, South Africa, dating to 58,000 years ago. Five of the specimens exhibit numerous red haematite stains which imply red ochre processing. Nevertheless, each artefact seems to have been used for a specific task. For example, the smallest grindstone was used for a combination of tasks—ochre, bone, and organic matter processing. The distinction between use residues, sediment contamination, secondary mineral formation, modern contamination, and components included in the sandstone that the grindstones are made from is discussed.

KEYWORDS

archaeometry, grindstones, Middle Stone Age, post-Howieson Poort, residues

1 | INTRODUCTION

1.1 | Grindstones in archaeological context

Used in the preparation of a variety of products, grindstones are interesting tools that can give information about behaviours that cannot be accessed from other classes of stone tools. Their porous surface allows the retention of abundant residues for the identification of material processing. The varied uses include plant (for food, fibres extraction, medicines, and poisons), faunal (for food, preparation of hides, polishing bone, antler, shell, and ivory), and inorganic material (preparation of stone tools, pigments, and clay for pottery) processing.[1] The earliest evidence for grinding technology is recorded in South Africa around 2.0 to 1.0 million years ago by early hominins for bone processing.[2] Grindstones have been discovered all over the world in many archaeological contexts. However, because of the relative rarity of these artefacts in archaeological assemblages and their low typological variability, grindstones have received little attention compared with other classes of lithic tools.

1.2 | Archaeological context: Sibudu

Situated above the uThongathi River in KwaZulu-Natal, South Africa, Sibudu is a large rock shelter occupied intermittently during the Middle Stone Age (MSA). Its different lithic technologies include pre-Still Bay, Still Bay, Howiesons Poort (HP), post-Howiesons Poort (post-HP), late, and final MSA. The estimated age of the Sibudu MSA sequence ranges between 77,000 and 38,000 years ago,[3] and the shelter was finally occupied during the Iron Age. A lot of information has been extracted about

MSA tool use at Sibudu, not only because of technological studies of the tools, but thanks to the remarkable preservation of residues on its stone tools.[4,5]

1.3 | Post-Howieson Poort—Sibudan

At Sibudu, the post-HP sequence (also called "Sibudu technocomplex" or Sibudan) is long and consists of many layers from Brown under Yellow Ash 2(i) (BYA2i) to Brown Speckled.[6] The estimated age of these layers at Sibudu is 58,500 ± 1,400 year ago;[7] they are associated with a savanna biome.[8]

The pointed lithic assemblage was produced using Levallois core preparation techniques, and it is characterised by elongated unifacial points with faceted platforms.[8] In comparison with other tools in the MSA sequence, the pointed ones are broader, thicker, longer, and heavier.[9] They seem more rudimentary compared with the previous industries which are Still Bay (with bifacial points) and HP (with backed, composite tools), but Conard and colleagues[10] point out that the Sibudan pointed assemblage is both diverse and sophisticated. Numerous other types of tools were also discovered such as blades, denticulates, hammerstones, and burins.[8] Many retouched tools made of hornfels and dolerite were also found such as scrapers bearing ochre and fat microresidues.[6]

The 58,000-year-old industry yielded the highest frequencies of grindstones (24 identified but maybe more can still be found in the collection) in the cultural sequence. They displayed various sizes and shapes, and the first macro- and microscopic observations[11] suggest the processing of various materials. In this new study, non-destructive and non-invasive analysis of a selection of the grindstones from the post-HP was performed using Raman microspectroscopy. It provided information about rock components, contaminants, and residues resulting from ancient uses. Optical microscopy was used in the first stage of analysis to identify areas of interest, but it also helped to detect the origin of each spectrum recorded (rock, residue, or contaminant).

2 | MATERIAL AND METHODS

2.1 | Samples

The material analysed here consists of six grindstones (made of sandstone) and associated sediments from several squares and layers containing the 58,000-year-old industry at Sibudu. They derive from Wadley's excavations between 2000 and 2008; these are being curated at the Evolutionary Studies Institute, University of the Witwatersrand, Johannesburg. Ranging here from the oldest to the youngest, the sediment layers concerned are Brown under Yellow Ash 2, Yellow Ash 2(i), Yellow Ash 2, Brown under Yellow Ash and Yellow Ash (YA) (see Wadley and Langejans[6] for more detailed stratigraphy). Table 1 lists the samples analysed. For the grindstone G23, the sediments were associated with the artefact, but other samples came from the same layer but not necessarily from the same square. The sediments associated with G8 and G22 (Brown under Yellow Ash and Yellow Ash in Brown under Yellow Ash 2, respectively) have unfortunately been used for other analyses. The samples were at all times handled with powder-free latex gloves to avoid any contamination from handling.

2.2 | Methods

2.2.1 | Optical microscopy

Microscopic images of the grindstones G19, G22, and G23 and their residues were obtained with an Olympus BX63 upright microscope setup in reflective light mode and recorded with CellSens Dimension software. The objectives used allowed for magnifications of 2×, 5×, and 10×. Because the samples have a rough surface and are not size-homogeneous, z-stacking was used to photograph the samples by combining all focal planes into a single focused image. As G1, G8, and G12 were too large to be observed with the Olympus BX63 (restriction of space between the stage and the objective), an Olympus SZ61 Stereo Zoom Microscope with LED illumination stand and equipped with an Olympus DP12 microscope digital camera system was used to obtain the pictographs of their surfaces.

2.2.2 | Raman micro-spectroscopy

A LabRam HR800 spectrometer (Horiba-Jobin Yvon) with an Olympus BX41 microscope attachment was used to characterise the molecular composition of the grindstones, their residues, and the sediments. Here, a 514.5 nm line of a Lexel argon ion laser allowed for measuring the majority of the components present without excessive fluorescence. However, a 784.3 nm diode laser (Sacher Lasertechick) was also used for some white, beige, and yellow microscopic areas on the grindstones resulting in fluorescence signal with the green line. Both radiations were focused through a 100× long working distance microscope objective (NA = 0.80) for the grindstones and a 100× microscope objective (NA = 0.90) for the sediments, from which a few milligrams were pressed between two glass slides to obtain a flat surface. Forty-five spectra were recorded on the sediment samples, and these give overall indication of their composition. Additional

TABLE 1 Descriptive and contextual details of the grindstones and sediments from the Sibudu 58,000-year-old layers (information in part extracted from de la Peña and Wadley[11])

Sample	Type	Layer	Square	Type of blank	Grindstone type	Fracture	Mass (g)	Length × width × thickness (cm)
G1	Gs	YA	B5a	Pebble	Faceted pebble	Y	104.3	5.0 × 6.0 × 2.5
SbS-YA-C6c	Sed	YA	C6c	—	—	—	—	—
SbS-YA-B4a	Sed	YA	B4a	—	—	—	—	—
G8	Gs	BYA	B5c	Pebble	Faceted cobble	N	>200	7.0 × 4.5 × 4.0
G12	Gs	YA2	B5a	Pebble	Round	Y	148.5	9.0 × 6.5 × 3.0
G23	Gs	YA2	C6c	Slab	Straight ridge	Y	99.6	10.8 × 4.0 × 1.5
SbS-G23-YA2	Sed	YA2	C6c	—	—	—	—	—
SbS-YA2-B4d	Sed	YA2	B4d	—	—	—	—	—
SbS-YA2-C5a	Sed	YA2	C5a	—	—	—	—	—
G19	Gs	YA2i	C4d	Pebble	Lozenge	Y	2	1.4 × 1.5 × 0.9
SbS-YA2i-C4	Sed	YA2i	C4	—	—			
G22	Gs	YA in BYA2	B5d	Pebble	Faceted pebble	N	22.6	3.8 × 2.2 × 1.6

Note. Gs = Grindstone; Sed = sediment; YA = Yellow Ash; BYA = Brown under Yellow Ash; YA2 = Yellow Ash 2; YA2i = Yellow Ash 2(i); BYA2 = Brown under Yellow Ash 2.

compounds might be present but not detected because of their low concentration or their Raman inactivity. The power at the sample was kept under 0.8 mW with the 514.5 nm laser and was around 1 mW with the 784.3 nm laser to avoid any thermal photodecomposition. The collection of the back-scattered Raman signal was performed using a 600 lines/mm grating (spectral resolution <2 cm^{-1}) and a charged coupled detector cooled with liquid nitrogen. The spectral range was between 95 and 1,900 cm^{-1} with the green line and 80–1,800 cm^{-1} with the 784.3 nm laser; when the presence of organic matter was suspected, a spectral window from 2,500 to 3,500 cm^{-1} was also measured. Different integration times were set depending on the point of analysis and the level of fluorescence, to obtain a correct signal to noise ratio.

3 | RESULTS AND DISCUSSION

3.1 | Rock composition

The grindstone samples are all made of sandstone (see Table 1), a material of choice for grinding purposes because of its high porosity and a relatively large grain size that creates a rough surface to allow reduction of various materials into a fine powder. A selection of Raman spectra attributed to the sandstone from which the grindstones are made is shown stack plotted in Figure S1. Some of these compounds can also have other origins which are discussed later. Table 2 summarises the results of the Raman analyses. The Raman bands at 110, 128, 151, 180, 200, 268, 287, 373, 404, 455, 476, 514, 655, 751, and 1,126 cm^{-1} are assigned to alkali feldspar (Figure S1c) and more specifically to the end member K-feldspars.[12] K-feldspars are common in sandstones,[13] and they were detected on specimens G12, G19, G22, and G23. For all the grindstones, multiple occurrences of quartz were recorded with its main band around 461–465 cm^{-1}. Quartz is also common in the sandstone composition[13] and was recorded alone (with its additional bands around 126, 206, 262, 354, and 391 cm^{-1}; see Figure S2) or in mixture with other compounds such as haematite, barite (main band at 988 cm^{-1}; Figure S1d), and amorphous carbon. Amorphous carbon is present everywhere on the tools. Carbonaceous materials are common in ancient rocks and come from bacterial activity (the hydrocarbon composing the cell membranes can be preserved or altered over time) or from abiotic precipitation from carbon-rich fluids.[14] Moreover, people made many fires in the archaeological site, and the carbon may equally derive from accidental contact with charcoal from fireplaces. All grindstones, except G8, revealed haematite with its main characteristic bands around 223, 293, 410, and 1,318 cm^{-1} (see spectra in Figure S1d). Haematite and manganese oxides (see Raman spectra in Figures 2, S3, and S5) could be geological inclusions in the sandstone because the colour of this sedimentary rock is influenced by iron and manganese oxides and other impurities.[13] Haematite, feldspar, gypsum (1,009 cm^{-1}; Figure S1f), barite, and clay minerals can act as cements in the sandstone composition. Gypsum occurs only on G1 and barite

TABLE 2 Summary of Raman spectra recorded on grindstone and sediment samples with their attributions

Sample component	G1	G8	G12	G19	G22	G23	SbS-G23-YA2	SbS-YA2-B4d	SbS-YA2-C5a	SbS-YA-C6c	SbS-YA-B4a	SbS-YA2i-C4	Agent of accumulation
Amorphous carbon	x	x	x	x	x	x	x	x	x	x	x	x	Sed and/or RC and/or UR
Haematite	x		x	x	x	x	x	x	x	x	x	x	UR and/or RC and/or Sed
Quartz	x	x	x	x	x	x	x	x	x	x		x	Sed and/or RC
Anatase	x		x	x	x	x	x				x		Sed and/or RC
Rutile	x			x		x							RC
Barite				x	x	x							SM and/or RC
Calcite				x		x							SM and/or RC
Gypsum	x												SM and/or RC
K-feldspar			x	x	x	x							RC and/or Sed
Na-feldspar				x				x					RC and/or Sed
Maghemite	x			x	x								UR and/or SM
Wüstite/iron oxides						x							SM or UR or LP
Manganese oxide		x	x			x							SM and/or RC
Lead chromate	x												UR or MC
Burkeite			x		x								SM
Bone	x			x			x	x	x		x	x	UR and Sed
Degraded organic matter				x							x		UR and/or Sed
Copper-phtalocyanate				x									MC
Fatty acid				x									UR or MC
Protein + Calcium nitrate			x										UR and/or SM and/or MC
Polyester fibre				x									MC

Note. LP = modifications due to laser thermal photodecomposition; MC = modern contamination; RC = rock component; Sed = sediments; SM = secondary mineral; UR = use residue.

on G19, G22, and G23. Barite can also be a secondary mineralisation product, and its presence suggests that the sample was exposed to crystallisation processes from ground fluids.[15] Notwithstanding possible geological inclusions, some of the haematite (and other substances) comprises residues that are clearly on top of the rock, rather than in it, and they seem to have derived from use of the grindstones.

Two titanium dioxides were detected on the grindstones. Rutile was recorded alone or mixed with other compounds in G1, G19, and G23; with bands at 145, 237, 448, and 611 cm^{-1} (Figure S1b). All grindstones showed the presence of anatase (Figure S1a) with the more intense band at 141 cm^{-1} and weaker features at 196, 396, 514, and 637 cm^{-1}. Anatase can arise from the mineralogy of quartz compacted sandstones. Anatase and rutile can also come from the crusts covering stone tools as it was the case for a palaeolithic industry from the southern Iberian Peninsula.[16]

The calcium carbonates recorded on G19 and G23 (sharp bands at 1,087 and 1,083 cm^{-1}, respectively; Figure S1e) may also come from the sandstone because calcite is a common occurrence in sedimentary, igneous, and metamorphic rocks.[17]

3.2 | Sediment analysis

Figure S2 presents a selection of Raman spectra obtained from the sediment samples. Another spectrum of feldspar (Figure S2d) was recorded for a sediment sample from layer Yellow Ash 2 and on the grindstone G19. The features observed are located at 149, 186, 209, 250, 270, 291, 327, 341, 413, 457, 478, 506, 762, and 815 cm^{-1}. The position of the strongest band (506 cm^{-1}) allowed classifying it as Na-feldspar, and the band positions are close to the spectrum of low albite recorded by Freeman and colleagues.[12] SbS-YA-B4a is the only sediment sample in which quartz (Figure S2a) was not detected. The presence of feldspars and quartz in the sediment is not surprising and most probably resulted from their formation process; for example, with rock fall from the roof of the rock shelter.

The PO_4 symmetric stretching vibration of bone around 961 cm^{-1} (Figure S2e) was detected for almost all sediment samples. A large quantity of burnt bone fragments was associated with hearths in the post-HP layers at Sibudu; they could have been burnt to avoid attracting carnivores or used as a fuel,[18] or the burning may have been accidental. Numerous spectra of amorphous carbon (e.g., Figure S2c) were recorded for all sediment samples on macro- and microscopic black areas with different sizes and shapes (sometimes fibres). For SbS-YA-B4a, a black fibre with an approximate diameter of 1 μm produced a spectrum showing two broad features between 1,150 and 1,700 cm^{-1} (Figure S2f). The band located in the highest wavenumbers exhibits a maximum intensity at 1,620 cm^{-1} and a shoulder around 1,584 cm^{-1}. A comparable spectrum was obtained on a similar fibre found on a Still Bay pointed tool from Sibudu,[19] and it was attributed to organic matter with incomplete combustion. All the sediments contained haematite (Figure S2b); the band positions and half width at half maximum are slightly different from the spectrum presented in Figure S1d because, for example, of the difference in crystal size and orientation, nonstoichiometry, and substitutions of some atoms. Sediments and particularly heated sediments often contain iron oxide.[19] There was extensive use of fire and ochre processing at Sibudu. These activities gave rise to the presence of concentrations of haematite and amorphous carbon in the sediments.

Gypsum, barite, calcium carbonate, and rutile are not present in the sediment samples, so they are more likely to be either rock inclusions or the result of secondary mineral formation.

3.3 | Residue analysis

The distinction between rock inclusions, sediment contaminants, and modern and ancient anthropogenic residues is important for understanding the tool uses. This issue was already discussed for the study of pointed stone tools from the Still Bay industry at Sibudu,[19] and performing optical microscopy on the samples is necessary for the discrimination.

3.3.1 | G1

Photographs of G1 and examples of micropictographs and representative Raman spectra detected on the grindstone are presented in Figure 1. Two spectra of gypsum were recorded for G1 (spectra not shown); and even though gypsum is common in Sibudu's sediments and grows as a secondary, postdepositional product,[6] it was not detected in the sediments analysed in this study. In Sibudu, its origin is not well understood, but Schiegl used Fourier-transform infrared spectroscopy to show that its occurrence is not linked to a specific type of sediment and can result from plant ash or bone apatite.[20] Only one spectrum showing the PO_4 stretching vibration of bone was recorded on G1, and it was mixed with quartz, haematite, and amorphous carbon (Figure 1d(D)), thus, we attribute its presence to contamination from sediments. Raman spectroscopy detected haematite all over the grindstone (Figure 1d(B, C & D)), that is, on the rounded edges and the central part. The macro- and microscopic observations revealed the presence of large

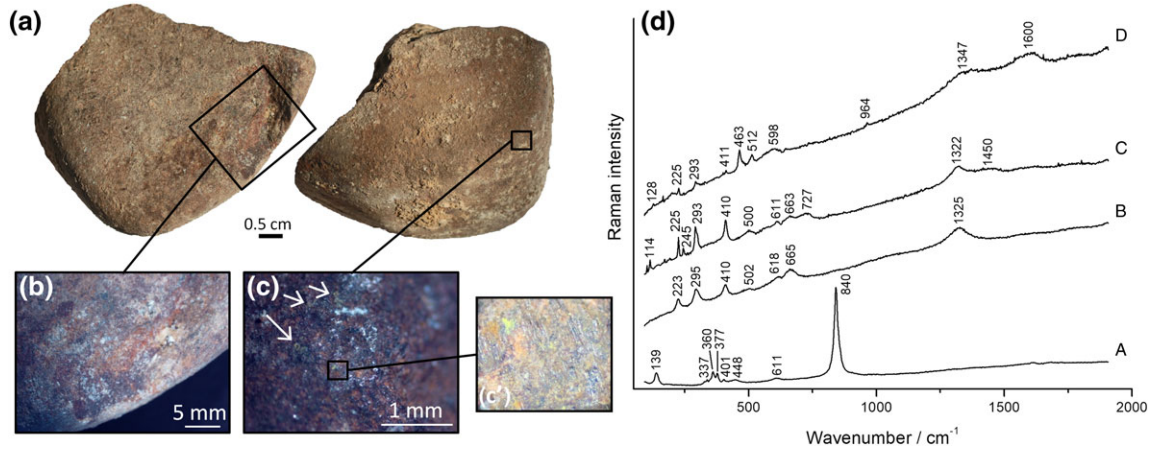

FIGURE 1 Macro- (a) and microphotographs (b, c & c′) of G1 and examples of Raman spectra (d) recorded on the grindstone; (A) crocoite and rutile, (B) haematite, (C) haematite and maghemite, and (D) quartz, haematite, bone, and amorphous carbon. (b) shows red and dark residues attributed to haematite that is sometimes mixed with maghemite. (c) and (c′) display the bright yellow residues (marked by the arrows) attributed to crocoite and striations observed on the edge of the grindstone. G1 is subrounded, and it has a fracture that split the grindstone. On the surviving round edge, smoothing, polish, and micro-striations can be seen [Colour figure can be viewed at wileyonlinelibrary.com]

red stains (see Figure 1b) composed of haematite; they most probably come from ochre processing. Sometimes, three additional features were recorded in combination with the haematite ones at 114, 727, and 1,450 cm^{-1} (Figure 1d(C)); these bands are assigned to maghemite (γ-Fe_2O_3). It is rare in the literature to find maghemite spectra with a spectral range below 150–200 cm^{-1}. However, in a study on maghemite nanoparticles, the heating under laser at 15 mW induced the formation of a band around 119 cm^{-1} before transformation into haematite.[21] Moreover, the Raman spectrum of synthetic maghemite published by Kuebler[22] exhibits an intense band at 114 cm^{-1} confirming the attribution of this band to maghemite. The broad band around 345 cm^{-1} is not observed for G1. This band is not always present in the spectra presented in the literature because maghemite has a weak response (spectra present a low signal to noise ratio even after long time acquisition) due to its poor scattering properties.[23] The most intense band of maghemite is asymmetrical, as observed by Neff and colleagues,[24] and is composed of a broad shoulder around 674–683 cm^{-1} (which is hidden by the haematite contribution in the spectrum presented in Figure 1d) and another broad component around 714–736 cm^{-1}. In the literature, the very broad band around 1,411–1,451 cm^{-1} does not appear all the time for maghemite spectra because this band is linked to magnetic properties of crystal grains.[24] Maghemite can come from different origins and is mainly obtained through heating iron oxides or oxyhydroxides. For example, maghemite can occur as a dehydroxylation product of lepidocrocite (γ-FeOOH)[22] and an oxidation product of magnetite (Fe_3O_4).[25] In both cases, maghemite is obtained at temperatures close to 200 °C, then the product is transformed to a mixture of maghemite and haematite at higher temperature, and finally to pure haematite. The metastability of maghemite with respect to haematite explains the presence of haematite bands in the spectrum, along with those of maghemite. The same process is observed with goethite (α-FeOOH) heated in the presence of organic matter.[26] Maghemite could thus be the product of heating iron oxides or oxyhydroxides present within the rock or from ochre residues on the rock surface.

Figure 1c, c′ show the presence of several bright yellow microresidues located on striations along the edge of the grindstone. The Raman analysis of these residues revealed the features of lead chromate ($PbCrO_4$) at 139, 337, 360, 377, 401, and 840 cm^{-1}[27] mixed with rutile (448 and 611 cm^{-1}; Figure 1d(A)). Lead chromate can have a natural and a synthetic origin. Lead chromate occurs naturally as the mineral crocoite in the form of crystals exhibiting a bright orange-red colour.[28] The streak is however orange-yellow, and when it is fine-grained; crocoite can be bright yellow as observed for the residue on G1. This mineral can be found in South Africa.[29] $PbCrO_4$ is also a synthetic pigment named chrome yellow and used by European painters from 1809.[30] Lead chromate was also detected as part of the composition of a yellow pigment on a coffin from Egyptian dynastic burials (~1600 BC), but the researchers pointed out that the residue may come from restoration processes.[31] Mixtures of lead chromate and rutile have

been detected on traffic paint samples in the USA.[32] The rutile present can also be a geological inclusion because it has been detected on two of the other grindstones (G19 and G23); the rutile band at 141 cm^{-1} is hidden under the lead chromate band at 139 cm^{-1}. It is not impossible that these residues originate from modern contamination, but the fact that they are pasted in striations of the grindstone is in good agreement with the grinding of crocoite. To our knowledge, this would be the earliest use of crocoite recorded. However, no clear evidence allows acceptance of one or the other hypothesis.

3.3.2 | G8

Raman analyses of G8 revealed the presence of only three compounds. Quartz and amorphous carbon were detected all over the grindstone and most probably come from sediment contamination and/or are from the rock composition. The sample displays numerous grey metallic stains located on all the facets with a size ranging from few micrometres to several centimetres (Figure 2a, b). These residues are specular when observed with stereo zoom microscope and LED illumination (Figure 2b). The main feature is very broad and consists of three maxima located around 662, 616, and 581 cm^{-1}; additional broad bands are observed at 503, 397, 200, and 150 cm^{-1} (Figure 2c). This spectrum is characteristic of manganese oxides and oxyhydroxides. Because of the large number of compounds that they can form in different oxidation states, manganese oxides are not straightforward to distinguish with Raman spectroscopy. Moreover, spectra of the same compounds vary depending on authors. Nevertheless, we can hypothesise that the spectrum obtained is a mixture of different manganese species. The band at 662 cm^{-1} is most commonly attributed to the Mn—O stretching vibration of pyrolusite (β-MnO_2)[33] or more generally to polymorphs of MnO_2.[34] All the other features are close to the hollandite-like ($(Ba,K)(Mn,Ti,Fe)_8O_{16}$) vibrational bands.[35] No manganese oxide pieces were discovered in the Sibudu cultural sequence, and no sources has been located around the site. The metallic grey areas present on each face of the stone may have originated from a biomineralisation process by bacteria, fungi, or algae rather than from manganese oxide processing. Manganese oxides were observed on bones from the HP and post-HP layers at Sibudu.[18] G8 is the heaviest of the grindstones found in the 58,000 years old layers and may have been used for a very specific task. One hypothesis is that it was used to the process organic material which degraded through time and promoted the formation of the manganese stains on its surface. No haematite

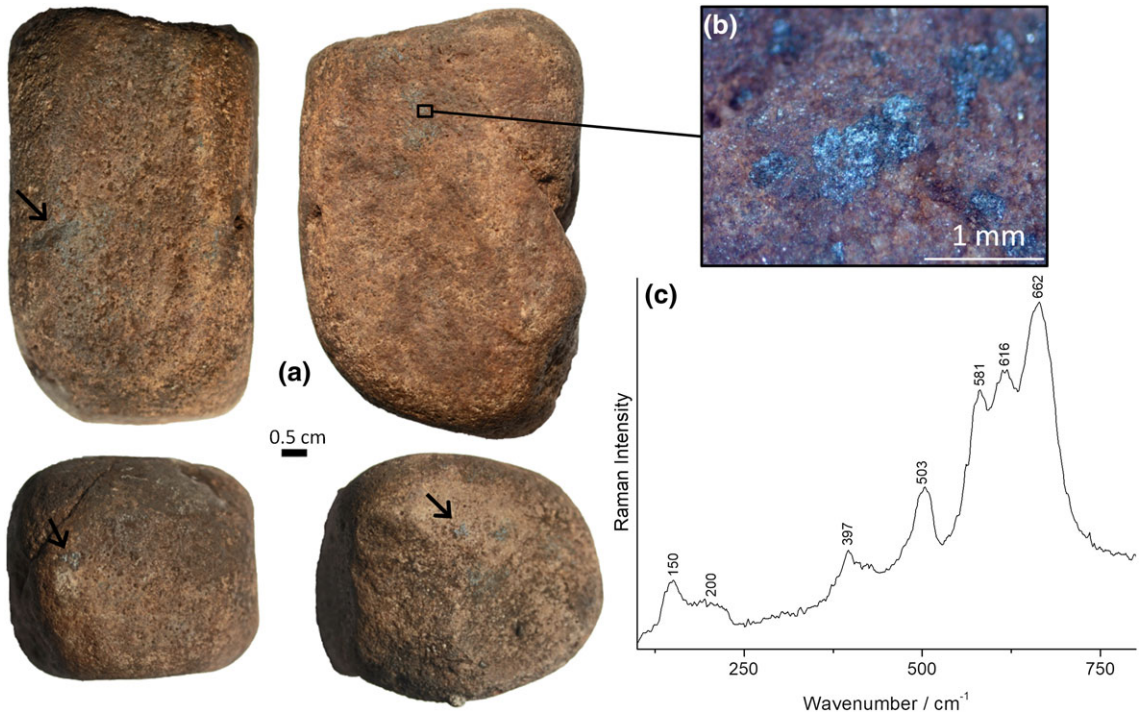

FIGURE 2 Macrophotographs of G8 (a), microphotograph (b) with an enlargement of one of the metallic-grey residues present all over the rock (the arrows in (a) are pointing to some examples of them) and characteristic Raman spectrum (c) of these residues attributed to manganese oxide. This faceted cobble shows some cracks measuring several centimetres and usewear traces such as smoothing on several facets and pitting [Colour figure can be viewed at wileyonlinelibrary.com]

occurrences were recorded on G8, and there is then little sediment contamination.

3.3.3 | G12

G12 exhibited multiple red stains (Figure S3A,B,C) attributed to haematite with Raman spectroscopy (Figure S3D(a)), especially on the smoothed and pitted use wear traces. As explained previously, the occurrences of anatase, amorphous carbon, and K-feldspar may derive from the sediments and/or the rock from which the grindstone is made. Another type of manganese oxide spectrum was recorded on a brown microscopic area located on the curved part of the grindstone (Figure S3D(c)). The large feature exhibits a component at 609 cm^{-1} with two shoulders around 649 and 707 cm^{-1} and three weaker bands at 493, 333, and 118 cm^{-1}. Inside the curved part of the grindstone, a spectrum suggesting a mixture was recorded (Figure S3D(b)). The bands at 1,059, 997, 631, 613, and 483 cm^{-1} are attributed to burkeite (Na_2CO_3,$2Na_2SO_4$).[36] Some of the bands show a slight shift compared with the spectra from Kornasov and colleagues,[36] and this is probably due to a difference in stoichiometry. The bands at 306 and 165 cm^{-1} could not be attributed. Burkeite is commonly described as a characteristic mineral in saline soils or continental lacustrine evaporite deposits, and more recently, it was found as a product of hydrothermal fluids and in melt inclusions in olivine.[36] It is also an eco-friendly alternative to phosphate carriers of detergent components. No detergent was used to clean the grindstones, so it is then most probably a deterioration product from the sandstone[37] or from residues present on it (e.g., carbonate formation can originate from the degradation of polysaccharides, including both cellulose and hemicelluloses and lignin). It is not impossible that plant processing introduced polysaccharides to the grindstone. On the edge of the grindstone, a spectrum was recorded showing features of organic matter with bands around the Amide I and III regions and in the νCH region (Figure S3D(d)). The features are broad, and they are unable to give a specific attribution. Moreover, a sharp band is observed at 1,052 cm^{-1} which can be attributed to calcium nitrate. As observed by Bordes and colleagues,[38] the calcium nitrate could arise from a degradation process that occurred postdepositionally. It is not impossible that the bands at 1,003 and 1,052 cm^{-1} originated from burkeite.

3.3.4 | G19

The smallest grindstone fragment analysed contains a large number of mineral and organic residues (Figure 3). Primary and secondary minerals possibly originating from rock and sediments were identified such as quartz, anatase, calcite, barite, rutile, K-feldspar, and amorphous carbon. The K-feldspar spectra were recorded on the

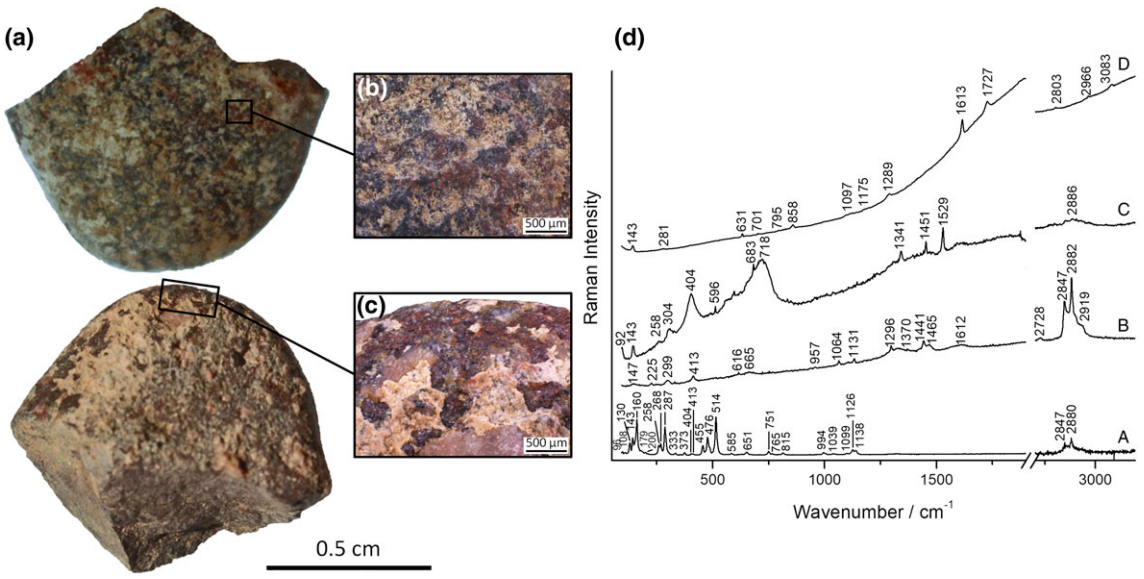

FIGURE 3 Macro- (a) and microscopic details on G19, (b) displays an enlargement of red residues present all over the rock attributed to haematite, and (c) on bone crust, pink crystal, and haematite residues; and characteristic Raman spectra (d) of organic matter recorded on the grindstone; (A) k-feldspar and organic matter, (B) saturated fatty acid, (C) copper-phtalocyanine, maghemite, and anatase, and (D) polyester fibre. G19 is the smallest fragment of grindstone in the collection; notice the rounded edges showing grinding striations [Colour figure can be viewed at wileyonlinelibrary.com]

pinkish crystals observable Figure 3c. One of them (Figure 3d(A)) is well defined with sharp bands and no fluorescence contribution. All the bands commonly described[12,39] are present, and supplementary features are noticeable. Well-ordered feldspars exhibit more bands than feldspars with a lower structural symmetry.[40] The literature does not present many spectra with a spectral range below 100 cm^{-1}, so the weak band at 96 cm^{-1} could be a characteristic feature of the low wavenumber range of feldspars. The band located at 143 cm^{-1} is most probably from anatase. Surprisingly, two bands were recorded in the C—H stretching region at 2,847 and 2,880 cm^{-1} showing the presence of organic matter.

Many red stains can be noticed at macro- and microscopic scales (Figure 3a,b,c). The red residues are smeared all over the rock with a higher concentration on the rounded edges exhibiting grinding striations. Raman analyses indicated the presence of haematite all over the grindstone; thus, ochre was one of the materials processed with grindstone G19. A white/beige crust is also spread all over the grindstone. The 514 nm laser excitation was not able to determine its composition because of a high contribution of the fluorescence effect. By using the 785 nm laser line, it was possible to identify the presence of bone with the band at 961 cm^{-1}. Bone was recorded on both sides of the grindstone; the stone was probably used to polish bone tools or for creating bone powder.

A spectrum of a degraded organic compound was recorded on the edge of the tool with large bands around 1,618 and 1,328 cm^{-1} (data not shown). It could result from the processing of burnt organic matter, or as explained previously, it might have come from sediment contamination. In the same area of the grindstone, a spectrum was recorded with organic matter features, especially in the ν(CH) region around 3,000 cm^{-1} (Figure 3d(B)). The shoulder around 2,919 cm^{-1} is attributed to $\nu(CH_3)$ symmetric; the intense sharp bands at 2,882 and 2,847 cm^{-1} to $\nu(CH_2)$ asymmetric and symmetric, respectively; and the weak band at 2,728 cm^{-1} to $\nu(CH_3—CH)$. The bands at 1,465, 1,441, 1,427 (shoulder), 1,370, and 1,296 are due to δ(CH2); ν(CC) bands are located at 1,130 cm^{-1} and ν(CO) at 1,064 cm^{-1}. In the lower wavenumber region, the band at 413 cm^{-1} arises from δ(CCC) and the bands at 299, 225, and 147 cm^{-1} from twisting vibrations of CH_3 and COH. All these bands are characteristic of long chain hydrocarbons, especially fatty acids.[38] The little spectral intensity in the 1,500–1,700 cm^{-1} region allows for attributing the spectrum to a saturated fatty acid (absence of C=C bonds). Fatty acids can originate from animal fat, vegetable oil, or wax. They can even appear from modern or past handling,[38] and distinguishing contamination due to modern handling and fatty acid microresidues due to ancient use or handling is not straightforward. Several microanalyses studies on other class of stone tools excavated from the post-HP layers at Sibudu—such as unifacial points and scrapers[6]—revealed the presence of fat often mixed with ochre, and the compounds could have been hafting adhesives, hide preparation mixtures, or residues on butchery tools. Another spectrum implying the presence of organic matter (Figure 3d(D)) was recorded on a twisted fibre measuring around 10 μm in diameter. The spectrum shows a high fluorescence level, but some bands can be distinguished at 2,803, 2,966 (νC—H), and 3,083 (ν=C—H) cm^{-1}. Other features can be observed at 1,727 (νC=O), 1,613 (νC=C), 1289 (δCH2), 858, 795 (δCCH), and 701 (νCC) cm^{-1} and are attributed to a polyester fibre.[41] This fibre originated from modern contamination (most probably from clothing). The organic residues are located around the K-feldspar crystals which may act as a niche for these residues.

A spectrum showing broad and sharp vibrational bands was detected on a black/brownish area again near a feldspar crystal (Figure 3d(C)). Copper-phtalocyanine was identified with the bands at 1,529, 1,451, 1,341, 683, and 596 cm^{-1}. α-, β- and ε-copper phthalocyanine are blue synthetic pigments and are widely used in modern artists' paints starting from the end of the 20th century.[42] This chemical compound definitely comes from modern contamination such as marker pen, maybe arising when marking the bag, as it was the case on French megalithic monuments.[43] These contaminating specks cannot be seen with the naked eye. The broad bands at 258, 304, and 718 cm^{-1} are attributed to maghemite and the sharp band at 143 cm^{-1} to anatase.

3.3.5 | G22

Figure S4 presents the results obtained for G22. The Raman spectra recorded on the sample and attributed to the rock, and sediments are the ones of quartz, anatase, amorphous carbon, and K-feldspar. Multiple stains showing a variety of red hues were observed on all the surfaces of the tool (Figure S4B,C). The Raman analyses of these stains identified the presence of haematite often mixed with maghemite and sometime barite (Figure S4D). A maghemite/haematite spectrum is associated with striations on the surface of the rock (Figure S4C). The spectrum showing a mixture of maghemite, haematite, and barite (Figure S4D(d)) also presents a band at 1,055 cm^{-1} which can be attributed to potassium nitrate or hydrated calcium nitrate; these soluble salts could have precipitated on the grindstone.[44] Only one

occurrence of maghemite was detected without the contribution of haematite (Figure S4D(c)); this spectrum is very similar to the one recorded by Kuebler [22] on synthetic maghemite with bands located at 114, 262, 297, 346, 375, 502, 640, 672, 724, 1,255, and 1,424 cm^{-1}. Another spectrum of burkeite was detected on G22 with slight shift of the wavenumbers (Figure S4D(a)). The band around 167 cm^{-1} is also present in the spectrum of G12, and it is assigned to the compound. As explained previously, the presence of burkeite is due to degradation processes.

3.3.6 | G23

Macro- and microphotographs of G23 and some of the Raman spectra obtained on the tool are presented in Figure S5. The Raman spectra attributed to the sediments and the rock are quartz, anatase, calcite, amorphous carbon, K-feldspar, and rutile. Numerous beige residues are visible on both sides of the grindstone (Figure S5A,B). Raman spectroscopy show that they comprise barite (Figure S5D(e)) and probably arise from a subsolidus alteration of a pre-existing primary mineral of the rock and/or the sediments. Haematite was detected everywhere on the tool (Figure S5D(d)). However, it was not possible to analyse the striated edge showing because of the limited space between the stage and the objective of the Olympus BX41 microscope. Several manganese oxide spectra were recorded on brownish/black areas of the tool. Two examples are shown in Figure S5D. The spectrum with a low fluorescence level and showing the features of amorphous carbon (Figure S5D(a)) exhibits bands at 385, 497, 577, and 644 cm^{-1}. Julien and colleagues[33] assigned the following three major features of birnessite-type MnO_2 peaking at 500–510, 575–585, and 625–650 cm^{-1}. Birnessites are phyllomanganates; they exhibit low crystallinity or have small sized crystals which can explain the broadness of the bands. The second spectrum exhibits bands at 400, 502, 583, 611, and 668 cm^{-1} (Figure S5D(b)), and these are very similar to the manganese spectra obtained on G8. They are thus attributed to the same species. A last spectrum was recorded on the red stain shown in Figure S5C. This area of the tool provided only a fluorescence signal except on black microscopic grains where amorphous carbon was recorded and on a yellowish/grey area where broad bands around 243, 329, 387, 648, and 1,306 cm^{-1} were detected (Figure S5 D(c)). The position of these bands seems to originate from a mixture of iron oxides. The band at 648 cm^{-1} can be attributed to wüstite (FeO). Wüstite is very unstable in open air because it comprises Fe^{2+}, and it can be found in corrosion layers in mixture with haematite and magnetite.[45] It is also sensitive to heat and then to laser exposure; above 570 °C, it transforms to haematite and magnetite.[25] The other bands present in the spectrum may then come from these compounds. The fact that this spectrum was recorded on the long red stain (maximum length and width of 2.8 and 0.35mm, respectively; Figure S3C) implies that it originated from human activity, yet it might alternatively be a secondary mineral or come from modifications due to laser thermal photodecomposition.

4 | CONCLUSION

When dealing with microresidue analyses, special care is needed to avoid modern and postdepositional contamination. Here, the spectra from copper-phtalocyanate and polyester were easily recognised as modern contamination. In the case of some organic (fatty acids) and mineral species (e.g., quartz, anatase, gypsum, burkeite, and manganese oxides), the distinction between natural geological inclusions, secondary mineral development, and modern or sediment contamination is often ambiguous. In the case of quartz, some authors have hypothesised that it can sometimes be an additive intentionally mixed into adhesive or pigment recipes,[46] though it can also be an unintentional inclusion in compounds from grinding ochre on sandstone.[47] In this study, the detection of quartz by Raman spectroscopy is attributed to the geological composition of the sandstone tools, sediment contamination, and ochre processing. Other mineral residues such as anatase, rutile, barite, burkeite, calcite, gypsum, and feldspar most probably originated from the sandstone from which the grindstones were made, from secondary mineralisation, or from sediment inclusions.

The results suggest that Sibudu's grindstones were used for various tasks, especially for grinding ochre. Haematite is detected on almost all of them; it is a component of reddish ochre. In Sibudu, people processed a lot of ochre especially in the 58,000 years old layers where 2,859 ochre pieces were discovered.[48] Moreover, another pigment with a bright yellow hue was present on one of the grindstones. This compound is a lead chromate and can have a natural occurrence in the form of the mineral crocoite. This pigment was first used as a synthesised product in the 19th century. Thus, if it is not a contaminant, its presence at Sibudu would mark the earliest use of a natural lead chromate pigment. The smallest grindstone fragment of the study revealed the presence of a white/beige crust made of bone spread on its entire surface, and the tool was thus probably used to polish bones or to create bone powder. Bone powder is edible but can also be used as a glue

component. The processing of bone supports an earlier microscopy study by Cochrane who detected animal residues on some of Sibudu's grindstone fragments.[49] On the same grindstone, organic compounds seem to have been processed; including fatty acid. This study adds more insights on the 58,000-year-old occupations at Sibudu when grindstones are a prominent feature of the lithic assemblages. It appears that subsistence strategies changed in comparison with earlier occupations where grindstones were rare or absent.

ACKNOWLEDGEMENTS

The author would like to acknowledge the Microscopy and Microanalysis Unit (University of the Witwatersrand) for the access to the optical microscope and the Raman spectrometer. I am grateful to the DST-NRF Centre of Excellence in Palaeosciences for financial support. Opinions expressed are those of the author and are not necessarily to be attributed to the Centre of Excellence in Palaeosciences. I am also very grateful to Dr Linda Prinsloo for her comments about the article. I thank Dr Héctor Morillas and Tomás Aguayo for taking a look at some of the spectra. Most of all, I would like to express my sincere gratitude to Prof Lyn Wadley, first for providing the grindstones, but also for the valuable comments made on this paper and for her continual encouragement, support, advice, and guidance.

ORCID

Marine Wojcieszak http://orcid.org/0000-0001-9508-4697

REFERENCES

[1] E. Hayes, PhD, University of Wollongong, **2015**.

[2] F. d'Errico, L. R. Backwell, *J. Archaeol. Sci.* **2003**, *30*, 1559.

[3] Z. Jacobs, R. G. Roberts, R. F. Galbraith, H. J. Deacon, R. Grün, A. Mackay, P. Mitchell, R. Vogelsang, L. Wadley, *Science* **2008**, *322*, 733.

[4] M. Lombard, *S. Afr. Archaeol. Bull.* **2004**, *59*, 37.

[5] P. Villa, L. Pollarolo, I. Degano, L. Birolo, M. Pasero, C. Biagioni, K. Douka, R. Vinciguerra, J. J. Lucejko, L. Wadley, *PLoS One* **2015**, *10*, e0131273.

[6] L. Wadley, G. Langejans, *S. Afr. Archaeol. Bull.* **2014**, *69*, 19.

[7] Z. Jacobs, A. G. Wintle, G. A. T. Duller, R. G. Roberts, L. Wadley, *J. Archaeol. Sci.* **2008**, *35*, 1790.

[8] M. Lombard, L. Wadley, J. Deacon, S. Wurz, I. Parsons, M. Mohapi, J. Swart, P. C. Mitchell, *S. Afr. Archaeol. Bull.* **2012**, *67*, 123.

[9] M. Mohapi, *S. Afr. Archaeol. Bull.* **2012**, *67*, 5.

[10] N. J. Conard, G. Porraz, L. Y. N. Wadley, *S. Afr. Archaeol. Bull.* **2012**, *67*, 180.

[11] P. de la Peña, L. Wadley, *PLoS One* **2017**, *12*, e0185845.

[12] J. J. Freeman, A. Wang, K. E. Kuebler, B. L. Jolliff, L. A. Haskin, *Can. Mineral.* **2008**, *46*, 1477.

[13] H. Morillas, J. García-Galan, M. Maguregui, I. Marcaida, C. García-Florentino, J. A. Carrero, J. M. Madariaga, *Spectrochim. Acta B* **2016**, *123*, 76.

[14] D. M. Bower, *J. Raman Spectrosc.* **2010**, *42*, 1626.

[15] S. E. Halcrow, J. Rooney, N. Beavan, K. C. Gordon, N. Tayles, A. Gray, *PLoS One* **2014**, *9*, e98462.

[16] V. Hernández, S. Jorge-Villar, C. Capel Ferrón, F. J. Medianero, J. Ramos, G. C. Weniger, S. Domínguez-Bella, J. Linstaedter, P. Cantalejo, M. Espejo, J. J. Durán Valsero, *J. Raman Spectrosc.* **2012**, *43*, 1651.

[17] H. G. M. Edwards, S. E. J. Villar, J. Jehlicka, T. Munshi, *Spectrochim. Acta A Mol. Biomol. Spectrosc.* **2005**, *61*, 2273.

[18] J. L. Clark, B. Ligouis, *J. Archaeol. Sci.* **2010**, *37*, 2650.

[19] M. Wojcieszak, L. Wadley, *Archaeometry* **2018**. https://doi.org/10.1111/arcm.12369

[20] S. Schiegl, P. Stockhammer, C. Scott, L. Wadley, *S. Afr. J. Sci.* **2004**, *100*, 185.

[21] Y. El Mendili, J.-F. Bardeau, N. Randrianantoandro, A. Gourbil, J.-M. Greneche, A.-M. Mercier, F. Grasset, *J. Raman Spectrosc.* **2010**, *42*, 239.

[22] K. E. Kuebler, *J. Geophys. Res. Planets* **2013**, *118*, 803.

[23] A. M. Jubb, H. C. Allen, *ACS Appl. Mater. Interfaces* **2010**, *2*, 2804.

[24] D. Neff, L. Bellot-Gurlet, P. Dillmann, S. Reguer, L. Legrand, *J. Raman Spectrosc.* **2006**, *37*, 1228.

[25] D. L. A. de Faria, S. Venâncio Silva, M. T. de Oliveira, *J. Raman Spectrosc.* **1997**, *28*, 873.

[26] M. P. Pomiès, G. Morin, C. Vignaud, *Eur. J. Solid State Inorg. Chem.* **1998**, *35*, 9.

[27] R. L. Frost, *J. Raman Spectrosc.* **2004**, *35*, 153.

[28] W. E. Ford, *Dana's textbook of mineralogy*, John Wiley and Sons, New York **1966**.

[29] M. J. Southwood, E. A. Viljoen, *Mineral. Mag.* **1986**, *50*, 728.

[30] L. Burgio, R. J. H. Clark, *Spectrochim. Acta A Mol. Biomol. Spectrosc.* **2001**, *57*, 1491.

[31] H. G. M. Edwards, S. E. Jorge Villar, K. A. Eremin, *J. Raman Spectrosc.* **2004**, *35*, 786.

[32] K. White, T. Detherage, M. Verellen, J. Tully, M. P. S. Krekeler, *Environ. Earth Sci.* **2014**, *71*, 3517.

[33] C. Julien, M. Massot, R. Baddour-Hadjean, S. Franger, S. Bach, J. P. Pereira-Ramos, *Solid State Ion.* **2003**, *159*, 345.

[34] F. Froment, A. Tournié, P. Colomban, *J. Raman Spectrosc.* **2008**, *39*, 560.

[35] C. M. Julien, M. Massot, C. Poinsignon, *Spectrochim. Acta A Mol. Biomol. Spectrosc.* **2004**, *60*, 689.

[36] A. V. Korsakov, A. V. Golovin, K. De Gussem, I. S. Sharygin, P. Vandenabeele, *Spectrochim. Acta A Mol. Biomol. Spectrosc.* **2009**, *73*, 424.

[37] B. Łydżba-Kopczyńska, J. M. Madariaga, *J. Raman Spectrosc.* **2016**, *47*, 1404.

[38] L. Bordes, L. C. Prinsloo, R. Fullagar, T. Sutikna, E. Hayes, Jatmiko, E. Wahyu Saptomo, M. W. Tocheri, R. G. Roberts, *J. Raman Spectrosc.* **2017**, *48*, 1212.

[39] V. Ciobotă, W. Salama, N. Tarcea, P. Rösch, M. E. Aref, R. Gaupp, J. Popp, *J. Raman Spectrosc.* **2012**, *43*, 405.

[40] P. Makreski, G. Jovanovski, B. Kaitner, *J. Mol. Struct.* **2009**, *924*, 413.

[41] L. Lepot, K. De Wael, F. Gason, B. Gilbert, *Sci. Justice* **2008**, *48*, 109.

[42] C. Defeyt, P. Vandenabeele, B. Gilbert, J. Van Pevenage, R. Cloots, D. Strivay, *J. Raman Spectrosc.* **2012**, *43*, 1772.

[43] A. Hernanz, M. Iriarte, P. Bueno-Ramírez, R. de Balbín-Behrmann, J. M. Gavira-Vallejo, D. Calderón-Saturio, L. Laporte, R. Barroso-Bermejo, P. Gouezin, A. Maroto-Valiente, L. Salanova, G. Benetau-Douillard, E. Mens, *J. Raman Spectrosc.* **2016**, *47*, 571.

[44] A. Tournié, L. C. Prinsloo, C. Paris, P. Colomban, B. Smith, *J. Raman Spectrosc.* **2011**, *42*, 399.

[45] R. K. S. Raman, B. Gleeson, D. J. Young, *Mater. Sci. Technol.* **1998**, *14*, 373.

[46] C. S. Henshilwood, F. d'Errico, K. L. van Niekerk, Y. Coquinot, Z. Jacobs, S.-E. Lauritzen, M. Menu, R. García-Moreno, *Science* **2011**, *334*, 219.

[47] L. Wadley, T. Hodgskiss, M. Grant, *Proc. Natl. Acad. Sci.* **2009**, *106*, 9590.

[48] T. Hodgskiss, *South Afr. Humanit.* **2012**, *24*, 99.

[49] G. W. G. Cochrane, *South Afr. Humanit.* **2006**, *18*, 69.

SUPPORTING INFORMATION

Additional Supporting Information may be found online in the supporting information tab for this article.

How to cite this article: Wojcieszak M. Material processed with 58,000-year-old grindstones from Sibudu (KwaZulu-Natal, South Africa) identified by means of Raman microspectroscopy. *J Raman Spectrosc*. 2018;49:830–841. https://doi.org/10.1002/jrs.5354